JOURNAL OF GEOPHYSICAL RESEARCH, VOL. 105, NO. D5, PAGES 6935–6944, MARCH 16, 2000

Effect of water vapor feedback on internal and anthropogenic variations of the global hydrologic cycle

Alex Hall[1]

Atmospheric and Oceanic Sciences Program, Princeton University, Princeton, New Jersey

Syukuro Manabe

Institute for Global Change Research/FRSGC, Tokyo

Abstract. Using two versions of the GFDL coupled ocean-atmosphere model, one where water vapor anomalies are allowed to affect the longwave radiation calculation and one where they are not, we examine the role of water vapor feedback in internal precipitation variability and greenhouse-gas-forced intensification of the hydrologic cycle. Without external forcing, the experiment with water vapor feedback produces 44% more annual-mean, global-mean precipitation variability than the one without. We diagnose the reason for this difference: In both experiments, global-mean surface temperature anomalies are associated with water vapor anomalies. However, when water vapor interacts with longwave radiation, the temperature anomalies are associated with larger anomalies in surface downward longwave radiation. This increases the temperature anomaly damping through latent heat flux, creating an evaporation anomaly. The evaporation anomaly, in turn, leads to an anomaly of nearly the same magnitude in precipitation. In the experiment without water vapor feedback, this mechanism is absent. While the interaction between longwave and water vapor has a large impact on the global hydrologic cycle internal variations, its effect decreases as spatial scales decrease, so water vapor feedback has only a very small impact on grid-scale hydrologic variability. Water vapor feedback also affects the hydrologic cycle intensification when greenhouse gas concentrations increase. By the 5th century of global warming experiments where CO_2 is increased and then fixed at its doubled value, the global-mean precipitation increase is nearly an order of magnitude larger when water vapor feedback is present. The cause of this difference is similar to the cause of the difference in internal precipitation variability: When water vapor feedback is present, the increase in water vapor associated with a warmer climate enhances downward longwave radiation. To maintain surface heat balance, evaporation increases, leading to a similar increase in precipitation. This effect is absent in the experiment without water vapor feedback. The large impact of water vapor feedback on hydrologic cycle intensification does not weaken as spatial scales decrease, unlike the internal variability case. Accurate representations of water vapor feedback are therefore necessary to simulate global-scale hydrologic variability and intensification of the hydrologic cycle in global warming.

1. Introduction

Because of the dependence of the saturation water vapor mixing ratio on temperature, as predicted by the Clausius-Clapeyron equation, anomalies of atmospheric water vapor tend to be correlated with surface-troposphere temperature anomalies. Since water vapor traps outgoing longwave radiation, this reduces the longwave radiative damping of the temperature anomalies. The reduction in radiative damping, in turn, increases the magnitude of the anomalies. This effect, generally known as water vapor feedback, has been recognized for some time [e.g., *Manabe and Wetherald*, 1967]. In a previous paper [*Hall and Manabe*, 1999] we estimated and compared the impact of water vapor feedback on internally generated temperature variability and global warming by analyzing coupled model simulations with and without water vapor feedback. In this article we analyze the same experiments, except that we focus on variations of the hydrologic cycle rather than temperature. It should be emphasized that in this article the term "water vapor feedback" refers only to this most generally known aspect of water vapor feedback: the interaction between water vapor and longwave radiation.

The importance of water vapor feedback to the variability of climate parameters other than temperature has received comparatively little attention. However, water vapor affects not only the outgoing longwave radiation at the top of the atmosphere but also the downward longwave radiative flux at the surface. For example, because of the increase in atmospheric water vapor associated with either an externally forced or internally generated warm surface-troposphere temperature anomaly, the emissivity of the atmosphere will increase, resulting in an increase in the downward longwave radiative flux at

[1]Now at Lamont-Doherty Earth Observatory of Columbia University, Palisades, New York.

Paper number 1999JD901172.
0148-0227/00/1999JD901172$09.00

the surface. A cold temperature anomaly would have the opposite effect, reducing downward longwave radiation at the surface. Longwave radiation, in turn, is a major component of the surface energy budget and therefore could have a large influence on the other components of the surface energy budget. For example, large variations in downward longwave radiation at the surface arising from water vapor feedback could lead to large variations in latent heat flux, or evaporation. This, in turn, would lead to significant variations in precipitation, particularly if the scale in question is the global scale, and atmospheric storage of water vapor is negligible.

To investigate whether the interaction between water vapor and longwave radiation makes an important contribution to both externally forced and internally generated global-mean precipitation variations in the manner hypothesized, we use a coupled ocean-atmosphere model, as noted above. A numerical model is a very flexible scientific tool because any physical mechanism it includes may be removed from the simulation, and the effect of the mechanism may be diagnosed. In this study we disable the water vapor feedback of the model by fixing the water vapor mixing ratios to their climatological mean values in the longwave portion of the radiative transfer subroutine. Thus anomalies in water vapor predicted by the hydrological component of the model have no effect on the atmosphere's longwave emissivity. We also employ a model configuration where water vapor is allowed to interact with longwave radiation, as the model was originally designed. By comparing the hydrologic cycle variability that results from unperturbed long-term integrations of the two model configurations with and without water vapor feedback (hereinafter referred to as the control and fixed H_2O configurations), we can assess the impact of water vapor feedback on the internally generated precipitation variability of the model. We can also manipulate the concentrations of greenhouse gases in a numerical model. Thus we can compare the hydrologic cycle intensification that results in the control and fixed H_2O configurations when CO_2 is gradually increased and then held fixed at twice its original value. These experiments allow us to see whether water vapor feedback impact on internally generated global-scale hydrologic cycle variations is similar to its impact on externally forced changes in the hydrologic cycle.

While some of the variability in water vapor mixing ratios may be a passive Clausius-Clapeyron-driven response to surface-troposphere temperature variability, water vapor also varies due to fluctuations of relative humidity. These water vapor anomalies cannot be understood in the framework of water vapor feedback. However, they could have a significant effect on downward longwave radiation and hence evaporation in the same manner as water vapor anomalies attributable to water vapor feedback. This effect would be included in the experiment with water vapor feedback but excluded from the one without. We will therefore verify in this paper that water vapor anomalies related to water vapor feedback are a major contributing factor to global hydrologic cycle variability, while water vapor anomalies that stem from relative humidity variability are not.

In the past, very little attention has been given to the mechanisms behind variability of the global hydrologic cycle, let alone the contribution of water vapor feedback. However, water vapor feedback has been mentioned as a contributor to hydrologic cycle intensification when greenhouse gases increase [*Manabe and Wetherald*, 1975; *Mitchell et al*., 1987] or solar constant is increased [*Wetherald and Manabe*, 1975]. Nonetheless, this is the first study to isolate water vapor feedback and examine its impact directly.

The presentation of this study is structured as follows: First, we give a detailed description of the numerical model (section 2) and the experimental technique (section 3) used in these simulations. In section 4 the analysis of water vapor feedback role in unperturbed precipitation variability is presented. In section 5 we examine the impact of water vapor feedback on the intensification of the hydrologic cycle when greenhouse gases increase. Finally, in section 6 we summarize and discuss our results.

2. Model Structure and Time Integration

The most important features of the model used for these experiments are described in some detail by *Manabe et al*. [1991]. It consists of a general circulation model of the world ocean coupled to an atmospheric general circulation model through exchange of heat, water, and momentum. The variables of the nine-vertical-level atmospheric component are represented in the horizontal by a series of spherical harmonics (rhomboidal truncation at zonal wavenumber 15) and corresponding grid point values (7.5° longitude by about 4.5° latitude grid box size). The radiative transfer calculation includes a seasonal cycle of insolation, though the diurnal cycle is not included. In addition, it takes into account the effects of clouds, water vapor, carbon dioxide, and ozone on both incoming and outgoing radiation, though only water vapor and cloud are actually predicted by the dynamical components of the model. At the land surface, the model computes budgets of snow, water, and heat. Soil moisture is parameterized using a "bucket" model: At every land surface grid point, water is accumulated through precipitation and depleted through evaporation in a bucket whose surface area is the same as the grid box. At any given time, if the water depth in the bucket exceeds 15 cm, runoff is predicted. Otherwise, soil moisture is given by the depth of the water in the bucket. Evaporation from the land surface, as predicted by the bulk aerodynamic formula, is reduced by the ratio of the depth of the bucket portion not occupied by water to the total depth of the bucket.

The finite-difference oceanic component, with a horizontal resolution of 4.5° latitude by 3.75° longitude and 12 vertical levels, uses the Modular Ocean Model (MOM) code described by *Pacanowski et al*. [1991]. This particular version of MOM is based, in turn, on a model described by *Bryan and Lewis* [1979]. In addition to horizontal and vertical background sub-grid-scale mixing, the model has isopycnal mixing, as discussed by *Redi* [1982] and *Tziperman and Bryan* [1993]. Convection occurs whenever the vertical stratification becomes unstable. Sea ice is predicted using a free drift model developed by *Bryan* [1969].

To prevent rapid climate drift that could distort the internally generated variability this study seeks to diagnose, the fluxes of heat and water obtained from the atmospheric component of the coupled model are modified by given amounts before they are imposed upon the ocean surface. While these "flux corrections" vary seasonally and geographically, they do not vary from year to year. Therefore they are unlikely to amplify or damp anomalies of sea surface salinity or temperature in a systematic way. Although the adjustments do not eliminate the shortcomings of the model [*Marotzke and Stone*, 1995], they do prevent rapid drift of the simulated climate from realistic initial conditions.

3. Experimental Design

As noted in section 1, this model was integrated in two configurations to test the effects of water vapor feedback. In both cases, water vapor is variable in the hydrologic component of the model, meaning that simulated clouds and precipitation are based on humidity values predicted by the model. In the control configuration the water vapor values predicted by the hydrologic component are passed to the longwave subroutine. In the fixed H_2O configuration, on the other hand, water vapor mixing ratios at all grid points and all nine vertical levels are fixed to their climatological mean, seasonally varying value in the longwave portion of the radiative transfer subroutine. The mean water vapor field used in the fixed H_2O experiments was calculated in the following way: First, integrating only the atmospheric component of the coupled model and using seasonally varying, climatological sea surface temperatures and sea ice as a lower boundary condition, the daily mean values of the entire water vapor field were saved away for 50 years. Then the values corresponding to any given day of the annual cycle were averaged over all 50 years of the integration, providing a mean water vapor field for every day of the year. These mean values were supplied to the coupled model longwave radiative transfer subroutine as the coupled integration proceeded through each day of the year. Since the mean climate of the control model is nearly identical to that of the atmosphere-only model, the mean water vapor field supplied to the longwave portion of the fixed H_2O model is also nearly identical to the mean water vapor field of the control model.

It should be emphasized that since water vapor was fixed only in the longwave radiative transfer subroutine of the fixed H_2O configuration, any feedback effects due to water vapor interaction with solar radiation are included in both configurations. The aspect of water vapor feedback relating to solar radiation is therefore not a subject of this study. For simplicity the term "water vapor feedback" refers only to the longwave feedback effects of water vapor throughout this article.

Imposing a mean water vapor field in the longwave code gives a greater greenhouse effect on average than allowing water vapor to vary. This occurs for two reasons. First, the dependence of the absorptivity of the atmosphere on specific humidity is approximately logarithmic, rather than linear. A positive moisture variation therefore produces a smaller anomaly in greenhouse trapping than a negative one of the same magnitude. The net effect is less greenhouse trapping when water vapor varies in the longwave. Second, the longwave code in the fixed H_2O model is not affected by the positive correlation between clear skies and dry air. The greenhouse effect attributable to water vapor is less when clouds are present and greater when they are absent. Therefore the increase in longwave absorption, which results from imposing the mean water vapor field on a dry cloudless sky, will be larger in magnitude than the decrease in absorption, resulting from imposing the mean water vapor field on a wet cloudy sky. The net impact is greater trapping when the mean water vapor field is imposed. These two effects would both result in a warmer fixed H_2O climate. A warmer mean climate could alter the unperturbed variability and sensitivity of the model without water vapor feedback, the subject of this and other studies stemming from these experiments. To eliminate this issue, different flux adjustments were imposed on the fixed H_2O model, ensuring that its mean climate is very similar to the control model.

The models were both integrated for 1000 years, long enough to provide extremely reliable and stable statistics. These integrations will be referred to as the unperturbed variability experiments. Although the flux adjustment technique described in section 2 minimizes climate drift, small trends remain in both experiments. For example, over the entire period of the 1000 year integration the fixed H_2O run exhibits a cooling trend of 0.009°C per century in global-mean surface temperature. A cooling trend of a similar magnitude exists in the 1000 year control run (0.035°C per century). For the purposes of the analysis of the unperturbed variability of the model, all such linear trends were first removed from the data. Using the same initial conditions as the unperturbed variability experiments, global warming experiments were also performed. Integrating the model in both configurations, CO_2 was increased at a rate of 1% per year until its concentration doubled, around year 70. Thereafter, it was fixed at the doubled value (720 ppm) for the remainder of the 500 year long experiments. The climate in such a model integration would likely continue to change at a slow rate for several centuries in response to the new CO_2 value if the integrations were continued beyond year 500. However, enough of the climate change has occurred by this point that we may consider the climate toward the end of these integrations to be broadly representative of the equilibrium response to the increase in CO_2. Thus to assess the impact of the doubled CO_2 value, the climate averaged over the 5th century of the global warming experiments was compared to the climate averaged over the 5th century of the unperturbed variability experiments. No trends were removed prior to this comparison, since any trend due to model drift should be identical in both the unperturbed variability and the global warming experiments.

4. Internally Generated Hydrologic Variability

Figure 1 shows the global-mean time series of annual-mean precipitation for the unperturbed control and fixed H_2O experiments. Comparison of the two time series indicates that there is significantly more global-mean precipitation variability in the experiment with water vapor feedback. This observation can be made more quantitative by comparing their standard deviations; the control standard deviation is about 50% larger than its fixed H_2O counterpart. This difference can be traced to the difference in variability of global-mean evaporation. Figure 2 shows these time series. As was the case with precipitation, the control experiment has more variability. In fact, the standard deviations of both evaporation time series are nearly identical to their precipitation counterparts, which suggests that variability in precipitation is directly linked to variability in evaporation. This hypothesis may be confirmed by calculating the correlation and linear regression coefficients between the precipitation and the evaporation time series, shown in Table 1 (row 1). Both the correlation and the regression coefficients are nearly one for the two experiments, indicating that a global-mean evaporation anomaly leads directly to a precipitation anomaly of the same sign and magnitude. Of course, this is a reasonable result, since it is unlikely that the model or real atmosphere could store significant anomalies of water vapor on timescales longer than a year. Thus the cause of the difference in precipitation variability in the two experiments must be rooted in the difference in the variability of evaporation. Now we explain why there is less evaporation variability in the experiment without water vapor feedback.

Water vapor influences the surface heat budget through its

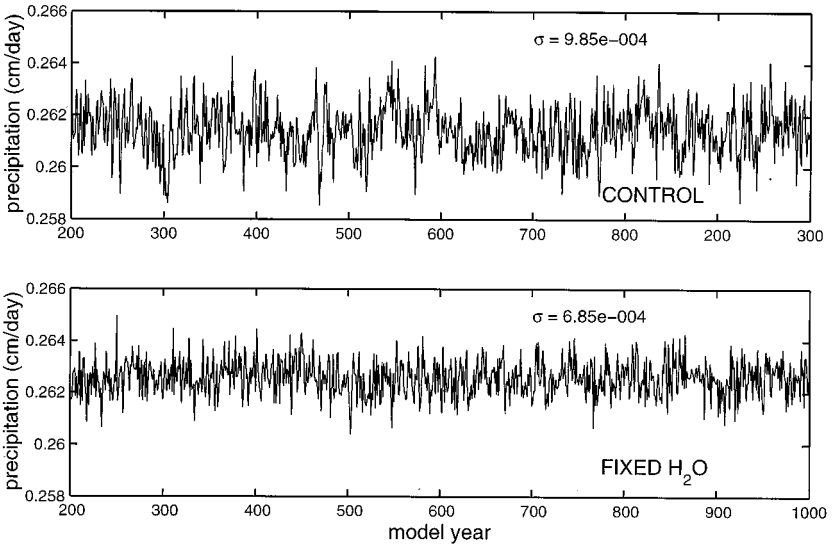

Figure 1. Global-mean time series of annual-mean precipitation for the control (top) and fixed H_2O (bottom) experiments. The standard deviation of each time series is also shown in the top right-hand corner of each panel.

effect on downward longwave radiation. Therefore we begin our analysis by examining the relationship between downward longwave radiation at the surface and surface temperature. Row 3 of Table 1 shows the correlation and regression coefficients between annual-mean, global-mean surface temperature and downward longwave radiation. In both cases, variability of surface temperature is closely tied to variability of downward longwave radiation; the correlation coefficients are both nearly one. This is because global-mean atmospheric temperature is very well correlated with global-mean surface temperature in both models. In addition, in the control model, global-mean water vapor anomalies, a significant contributor to atmospheric emissivity, also fluctuate in phase with surface temperature. For example, the correlation between annual-mean, global-mean water vapor averaged over the entire atmosphere and surface temperature is 0.71. When global-mean water vapor is averaged over the lower troposphere (850–1013 hPa), the part of the atmosphere most important for downward longwave radiation at the surface, the correlation with surface temperature is even higher (0.77). In addition, *Hall and Manabe* [1999] also showed that the regression between relative humidity and surface temperature in the control model is very close to zero throughout the atmosphere. Not only does global-mean atmospheric water vapor fluctuate in phase with surface temperature but it also fluctuates so as to approximately conserve relative humidity. In the control model, the simultaneous global-scale variations of surface temperature, atmospheric temperature, and absolute humidity, especially in the lower troposphere, make for a very tight correlation between downward longwave radiation and surface temperature.

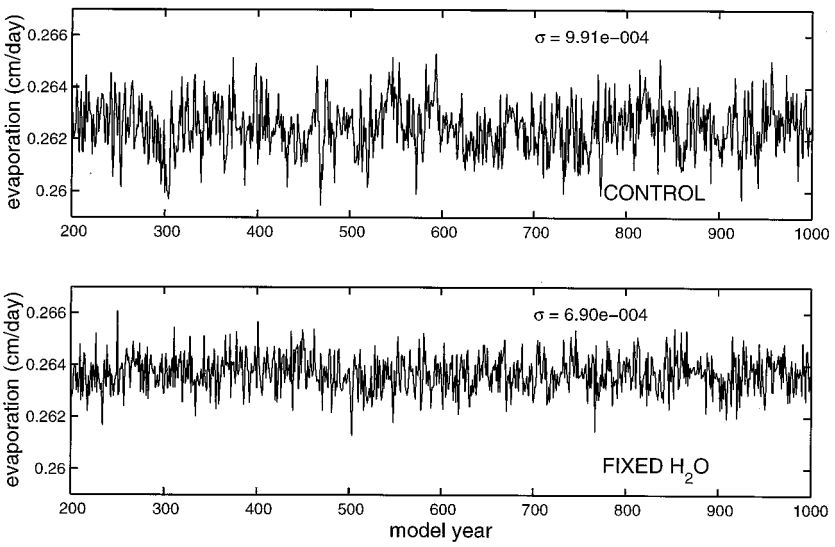

Figure 2. Global-mean time series of annual-mean evaporation for the control (top) and fixed H_2O (bottom) experiments. The standard deviation of each time series is also shown in the top right hand corner of each panel.

Table 1. Correlation and Regression Coefficients Between Various Time Series Listed in Column 1

Y/*X*	Correlation	Regression	Experiment
Precip./evap	0.99	0.99	control
(nondimensional)	0.99	0.98	fixed H_2O
Down lw./T^*	0.97	6.37	control
(W m^{-2} °C^{-1})	0.95	5.31	fixed H_2O
Lt. Ht./T^*	0.48	0.91	control
(W m^{-2} °C^{-1})	0.10	0.17	fixed H_2O
Sens. Ht./T^*	0.56	0.64	control
(W m^{-2} °C^{-1})	0.43	0.67	fixed H_2O
Net up. lw./T^*	−0.83	−0.13	control
(W m^{-2} °C^{-1})	0.77	1.57	fixed H_2O
Net down. sw./T^*	0.63	1.56	control
(W m^{-2} °C^{-1})	0.65	2.10	fixed H_2O

Variables taken as the dependent variable in the regression calculation are listed first, followed by the independent variable. T^* stands for surface temperature. Dimensions are also listed for the regression coefficient. All calculations are based on annual-mean, global-mean data from the last 800 years of the unperturbed integrations.

The water vapor feedback process described above creates an important difference in the regression coefficients listed in Table 1, row 3: A given surface temperature anomaly in the control experiment is associated with an anomaly in downward longwave radiation that is about 1 W m^{-2} larger than in the fixed H_2O case. This is because a warm (cold) surface temperature anomaly leads to an increase (decrease) in the opacity of the atmosphere through an increase (decrease) in atmospheric water vapor, resulting in a larger increase (decrease) in the radiation trapped and redirected toward the surface than in the experiment without water vapor feedback. The smaller downward longwave radiation anomaly in the fixed H_2O experiment is less effective in counterbalancing the upward longwave radiation anomaly given by the Stefan-Boltzmann law. Thus the total damping of the temperature anomaly due to net longwave radiation is larger in the fixed H_2O experiment.

Of course, the relationship between absolute humidity and surface temperature in this model may be different from the real climate. For example, *Sun and Held* [1996] showed that the regressions and correlations between tropical mean humidity and temperature in a model nearly identical to the present model are greater than in the rawinsonde data. According to their results the main discrepancy between model and observations is in the tropical middle to upper troposphere. However, as noted above, downward longwave radiation at the surface (the critical variable for this study) is influenced mainly by variations in lower tropospheric humidity. In this part of the atmosphere, interannual variations in water vapor are tightly controlled by surface temperature in both the model and the real world. In fact, whether the region in question is the tropics, the Northern Hemisphere, or the entire globe, the relationship between lower tropospheric humidity and surface temperature is the least controversial aspect of the water vapor feedback problem [*Dickinson et al*., 1996]. Thus the substantial increase in the regression between downward longwave radiation at the surface and surface temperature when water vapor is allowed to interact with longwave radiation in the control experiment is not unreasonable.

Since the damping due to net longwave radiation at the surface is larger in the fixed H_2O experiment, less energy is available for damping through latent heat flux. Surface temperature anomalies therefore ought to be less strongly associated with evaporation anomalies. This may be confirmed by examining the regression and correlation coefficients between annual-mean, global-mean surface temperature and latent heat flux (Table 1, row 5). They indicate that surface temperature and evaporation anomalies are much better correlated in the control experiment than in the fixed H_2O. In addition, the typical magnitude of a latent heat anomaly associated with a surface temperature anomaly, given by the regression coefficient, is also much larger in the control case. This effect, coupled with the fact that the variability of global-mean surface temperature itself is significantly larger in the control experiment (ratio of standard deviation, control/fixed H_2O = 1.53), explains the suppression of evaporation variability in the experiment without water vapor feedback.

To obtain a more complete picture of how water vapor feedback affects the surface energy budget, we examine the typical changes in the components of the surface energy budget which take place as surface temperature varies. These are given by the regressions listed in Table 1 (rows 5–11) and are also summarized in a bar chart (Figure 3). This chart illustrates visually why global-mean surface temperature anomalies are associated with larger evaporation anomalies in the control experiment. To facilitate understanding of this figure, we will

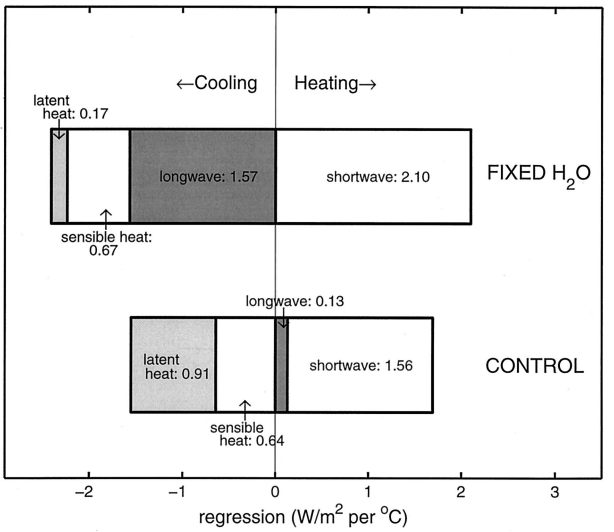

Figure 3. Stacked bar plot representation of the regressions among global-mean, annual-mean surface heat fluxes, and surface temperature for the fixed H_2O and control cases. All components of the surface energy budget are shown, including shortwave and longwave radiation, latent, and sensible heat. If a component of the surface energy flux changes so as to increase the amount of energy absorbed by the surface when surface temperatures are warm, it is placed on the right-hand (heating) side of the plot. Conversely, if it changes so as to decrease the energy absorbed by the surface when surface temperatures are warm, it is placed on the left-hand (cooling) side. Each component is labeled along with the numerical value of its regression with surface temperature. The longwave components are dark shaded, and the latent heat components are light shaded for emphasis. Although the surface heat budget is in balance at all times in this model, the various components of the surface heat budget do not balance perfectly in this plot. This is because the components are not perfectly correlated with temperature, and the regressions therefore do not reflect the entire surface heat budget.

take the example of a warm surface temperature anomaly and discuss how the components of the heat budget respond to it.

Figure 3 indicates that a global-mean warm surface temperature anomaly is associated with an increase in net downward solar radiation of the same sign and about the same magnitude in both experiments. This is due mainly to a decrease in sea ice and snow cover. In the fixed H_2O experiment this increase is balanced primarily by damping due to net longwave radiation. While increases in both upward and downward longwave radiation accompany the surface temperature increase, the upward flux increases much more than the downward flux. This is because the increase in water vapor associated with the warm temperature anomaly does not affect downward longwave radiation. The increase in solar radiation is also balanced to a lesser extent by sensible and latent heat fluxes. In the control experiment the increase in solar radiation is partly balanced by cooling through a sensible heat flux similar to that seen in the fixed H_2O experiment. Thus there is no difference in the damping of surface temperature through sensible heat flux. The substantial longwave damping seen in the fixed H_2O experiment does not occur when water vapor is allowed to interact with longwave radiation. In the control case, the increase in upward longwave radiation is balanced nearly perfectly by an increase in downward longwave radiation. The damping of the temperature anomaly must be accomplished instead through latent heat flux.

In section 1 we noted that anomalies of water vapor, which can be attributed to fluctuations of relative humidity and not to water vapor feedback, could also contribute to downward longwave radiation variability and hence evaporation and precipitation variability in the control experiment. However, the excellent correlation between global-mean downward longwave radiation and surface temperature shown in Table 1, row 3, implies that water vapor anomalies that are uncorrelated with surface-troposphere temperature anomalies (i.e., anomalies of relative humidity) do not play an important role in global-mean downward longwave radiation variability. Thus the difference in global-mean evaporation variability between the two experiments can be attributed almost exclusively to water vapor feedback, the mechanism documented in this section.

We have shown that the interaction between longwave radiation and water vapor is responsible for a considerable amount of global-scale hydrologic cycle variability; we now examine its impact as spatial scales decrease. Table 2 shows the control/fixed H_2O ratio of standard deviation of annual-mean evaporation and precipitation time series averaged over various regions, listed in order of decreasing size. It is clear from Table 2 that water vapor feedback does affect evaporation variability on spatial scales smaller than the global scale. For example, there is ~20–30% more hemispheric evaporation variability in the control experiment (rows 3 and 4). In general, however, the impact of water vapor feedback on evaporation variability decreases drastically as the size of the region decreases. On the grid scale (row 11), for example, there is on average only a 4% enhancement of evaporation variability due to water vapor feedback.

This spatial-scale dependence arises from the fact that water vapor feedback itself weakens as spatial scales decrease. *Hall and Manabe* [1999] showed that the regressions between atmospheric water vapor and surface temperature in this simulation decrease substantially as spatial scale decreases. This weaker water vapor feedback translates into a much smaller impact on the surface heat budget and hence latent heat release. The impact of downward longwave variability on grid-scale evaporation variability (row 11) may also be reduced in oceanic regions because any local longwave heating of the mixed layer may be balanced by advective heat exchange within the ocean as well as latent heat, sensible heat, and solar radiation. This effect is clearly less important as spatial scales increase, partially accounting for the much larger ratios for all the ocean (row 2) and hemispheric (rows 3 and 4) regions. It is also clear from a comparison of rows 2 and 5 in Table 2 that the impact of water vapor feedback on evaporation variability is smaller over land than over ocean. This is because water vapor feedback itself is relatively weak over dry land, where moisture is relatively unavailable; the regressions between water vapor and surface temperature (not shown) are on average substantially smaller over land than over ocean.

Table 2. Ratio (Control/Fixed H_2O) of Standard Deviation of Evaporation and Precipitation Time Series Averaged Over the Regions Indicated

Region	Evaporation	Precipitation
Global	1.44	1.44
All ocean	1.41	1.17
N. Hemisphere	1.27	1.21
S. Hemisphere	1.21	1.25
All land	1.07	1.05
Eurasia	1.00	1.01
Africa	1.15	1.05
N. America	0.87	0.98
S. America	1.07	1.13
Australia	1.06	1.11
Local	1.04	1.02

Row 11 shows the global mean of the ratio calculated at each grid point. All calculations are based on annual-mean data from the last 800 years of the unperturbed integrations.

The global scale also differs from smaller scales in that the atmospheric water budget at smaller scales is not a simple balance between evaporation and precipitation. Even if the interaction between longwave radiation and water vapor did enhance evaporation variability by the same amount on all spatial scales, these evaporation anomalies would not necessarily translate into precipitation anomalies of the same magnitude at the same location, since moisture anomalies, especially on very small spatial scales, may be easily advected by the atmospheric circulation. Thus while global-mean evaporation and precipitation variability are enhanced by the same ratio at the global scale, the ratios are different for all smaller scales. In general, however, the precipitation ratios, as their evaporation counterparts, decrease drastically as spatial scales grow smaller.

5. Hydrologic Cycle Intensification

In section 4 we illustrated how the interaction of water vapor and longwave radiation affects precipitation variability. We now turn our attention from internally generated variability to externally forced climate change. In addition to causing global warming, an increase in CO_2 is projected to lead to a global-scale increase of around 10 to 20% in both evaporation and precipitation. Readers interested in a detailed characterization of this hydrologic cycle intensification should consult *Kattenberg et al*. [1996] and *Mitchell et al*. [1990]. In this section we show that water vapor feedback is responsible for most of the

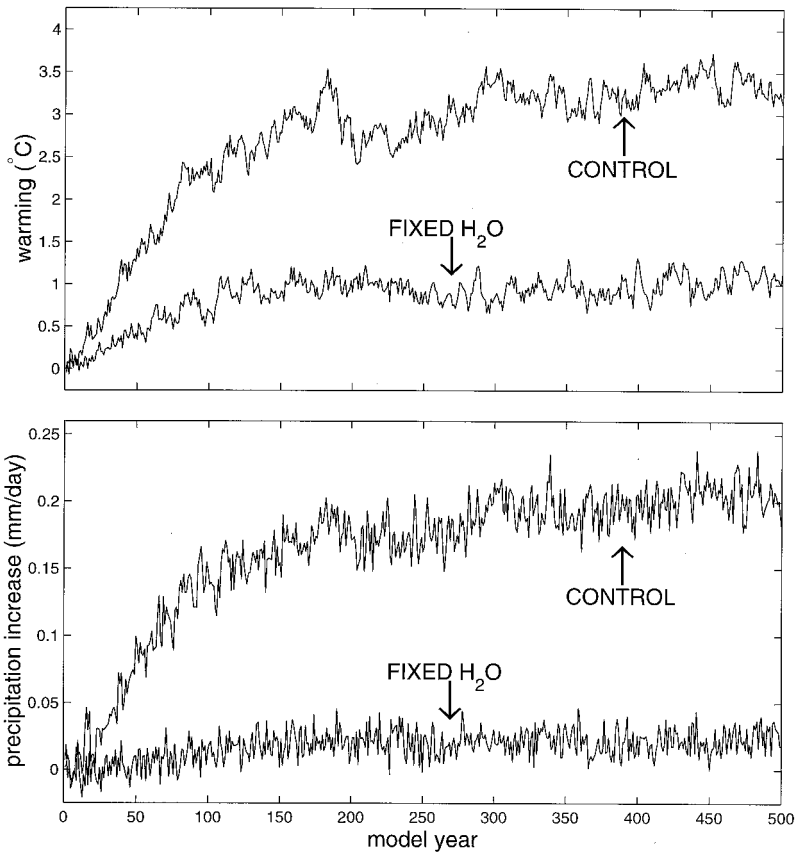

Figure 4. (top) The 500 year annual-mean time series of the global-mean surface temperature change in the global warming experiments relative to the unperturbed variability experiments. (bottom) As in the top panel except for precipitation rather than surface temperature.

intensification of the hydrological cycle that this model simulates in a global warming scenario.

As background to this discussion, we describe briefly the global-mean temperature change that occurs in both global warming experiments (see Figure 4, top). In both the fixed H_2O and the control cases there is a steady warming for the first 70 years. After CO_2 is fixed at year 70, the warming continues but at a much slower rate for the remainder of the experiments. Averaged over the fifth century, the global warming is 3.38°C in the control case. The fixed H_2O warming is about 3 times smaller, 1.05°C. The increase in absolute humidity that occurs as the climate warms, and which is responsible for this difference in sensitivity, is characterized by very little change in relative humidity [see *Hall and Manabe*, 1999, Figure 4].

Accompanying the increase in temperature is a steady increase in global-mean precipitation over the course of the control global warming experiment, shown in Figure 4, bottom. By the 5th century the precipitation increase reaches a value of 0.20 mm d^{-1}. Meanwhile, the increase in hydrologic cycle intensity in the fixed H_2O experiment is barely perceptible. Averaged over the 5th century, the precipitation increase in this case is only 0.023 mm d^{-1}, about an order of magnitude smaller than its control counterpart. Thus the impact of water vapor feedback on the externally forced precipitation increase is much larger than its impact on global warming; the increase in precipitation per degree surface warming is 3 times as large in the control experiment (0.061 mm d^{-1} $°C^{-1}$ versus 0.022 mm d^{-1} $°C^{-1}$). We devote the remainder of this section to explaining how water vapor feedback is responsible for this disproportionate increase in hydrologic cycle intensity.

In section 4 we saw that global-mean evaporation and precipitation variability are very tightly linked. Similarly, the increases in precipitation in the two global warming experiments take place in conjunction with identical increases in evaporation. The problem of explaining the weak enhancement of the hydrological cycle in the fixed H_2O global warming experiment therefore amounts to demonstrating why the increase in evaporation is so small compared to the control case. To carry out this analysis, we performed calculations that are the global warming analog to the regressions presented in Table 1, based on internal variability. To quantify the relationship between changes in variables X and Y in a global warming context, we first calculated global-mean differences in X and Y between the global warming and the unperturbed experiments averaged over the 5th century of both integrations. We then divided the difference in Y by the difference in X.

Using this technique, we examine the relationship between downward longwave radiation and surface temperature. In both fixed H_2O and control cases, downward longwave radiation increases because of the higher CO_2 concentration and higher atmospheric temperatures, which are themselves the consequence of the CO_2 increase. However, when the increased water vapor mixing ratios associated with the warmer climate are allowed to interact with longwave radiation, they augment the increase in downward longwave radiation: In the

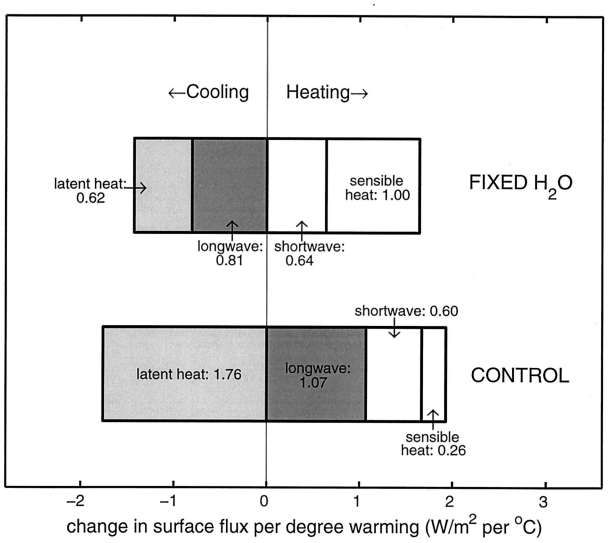

Figure 5. Stacked bar plot representation of the changes in global-mean surface heat fluxes per degree global-mean surface warming for the fixed H_2O and control cases. All components of the surface energy budget are shown, including shortwave and longwave radiation, latent, and sensible heat. If a component of the surface energy flux changes so as to increase the amount of energy absorbed by the surface upon global warming, it is placed on the right-hand (heating) side of the plot. Conversely, if it changes so as to decrease the energy absorbed by the surface, it is placed on the left-hand (cooling) side. Each component is labeled along with the numerical value of its change per degree warming. The longwave components are dark shaded and the latent heat components are light shaded for emphasis. The small net heating in both experiments reflects the slow warming that occurs over the course of several centuries after CO_2 reaches its doubled value at year 70 (see Figure 4).

fixed H_2O experiment the increase in downward longwave per degree surface warming is 5.16 W m^{-2} °C^{-1}, whereas in the control case, it reaches a value of 6.92 W m^{-2} °C^{-1}. Thus for every degree of surface warming, there is 1.76 W m^{-2} °C^{-1} more energy available at the surface in the control experiment.

To illustrate how this effect interacts with the other components of the surface heat budget, including latent heat, we present in Figure 5 a stacked bar chart similar to Figure 3. This chart summarizes the global-warming-related changes in the surface heat budget per degree warming in each experiment, calculated using the technique described above.

In both fixed H_2O and control cases the net downward shortwave increases in the doubled-CO_2 climate by a little more than 0.6 W m^{-2} °C^{-1}. This is mostly due to decreased sea ice and snow cover. Although shortwave radiation increases as temperature increases in both the unperturbed variability and in the global warming cases, the regressions between shortwave radiation and surface temperature are larger in the unperturbed variability case (see Figure 3). This is because internally generated interannual variability tends to be dominated by contributions from land and high-latitude locations [*Hall and Manabe*, 1999]. Since albedo feedback is a particularly strong factor in variability at high latitudes, the regressions between surface temperature and shortwave radiation are quite large. Although there is polar amplification of global warming, the warming is large enough in the tropics that the change in shortwave per degree warming is smaller in the global warming case.

In contrast to the unperturbed variability case, where sensible heat acts to cool the surface (see Figure 3), the net upward sensible heat flux decreases in both cases, leading to a net heating of the surface. This occurs because the increase in surface temperature leads to an increase in saturation vapor pressure at the surface. This in turn facilitates damping through evaporation, reducing damping through sensible heat flux. This systematic change in the Bowen ratio is absent in the unperturbed variability experiments. The fact that internally generated global-mean temperature anomalies are dominated by contributions from land and high latitudes in this model, while global warming is distributed more uniformly between land and ocean, may also account for the greater damping due to sensible heat flux in the unperturbed variability case.

The unperturbed variability and global warming cases are similar when the longwave component of the surface energy budget is considered. In the control global warming experiment, net upward longwave actually decreases, since the increase in downward radiation is larger than the increase in upward longwave radiation arising from CO_2-induced warming of the surface. Conversely, in the fixed H_2O global warming experiment, the increase in upward longwave owing to the surface temperature increase competes with a smaller increase in downward longwave radiation. Thus the balance is tilted toward cooling the surface.

This difference has profound consequences for the change in latent heat flux. In the experiment with water vapor feedback, all changes in components of the surface heat flux, with the exception of latent heat, act to heat the surface. This heating is balanced by a very large increase in latent heat flux to the atmosphere. On the other hand, in the experiment without water vapor feedback, even though the sum of the heating contributions of sensible and shortwave is larger than the control case, the fact that longwave radiation acts to cool rather than heat the surface means that the increase in latent heat flux has to be much smaller. Thus the mechanism for the weak intensification of the hydrologic cycle in the fixed H_2O global warming experiment is very similar to the mechanism for suppression of internally generated precipitation variability. These results are consistent with the work of *Wetherald and Manabe* [1975] who also noticed a decrease in net upward longwave radiation when they examined the response of a simplified atmosphere-only model to 2% increase of the solar constant. They also identified this decrease as one of the main reasons for the disproportionate increase in hydrologic cycle intensity in their perturbed climate.

In section 4 we examined the spatial-scale dependence of the impact of water vapor feedback on hydrologic variability. As a counterpart to that discussion, we examine the effect of water vapor feedback on hydrologic cycle intensification at spatial scales smaller than the global scale. Table 3 shows the control/fixed H_2O ratio of the evaporation and precipitation changes due to CO_2 doubling averaged over various regions. The changes are defined as the 5th-century-mean difference between the global warming and unperturbed variability experiments. The regions are listed in order of decreasing size, just as in Table 2. Examining the evaporation ratios, it is clear that there is no systematic spatial scale dependence of the impact of water vapor feedback. This contrasts with the internal evaporation variability case, where water vapor feedback impact decreases as spatial scale decreases. This occurs because the

Table 3. Ratio (Control/Fixed H_2O) of Evaporation and Precipitation Changes That Take Place by the 5th Century of the Global Warming Experiments Averaged Over the Regions Indicated

Region	Evaporation	Precipitation
Global	8.9	9.0
All ocean	8.7	12.5
N. Hemisphere	10.2	8.2
S. Hemisphere	7.9	10.4
All land	9.5	5.6
Eurasia	7.3	4.3
Africa	63.2	−7.6
N. America	16.9	5.5
S. America	11.7	5.6
Australia	3.5	−8.5

Negative values indicate a decrease in precipitation in the experiment without water vapor feedback.

warming itself is global in scale and relatively uniform geographically, as is its associated water vapor feedback. The very large ratio in the case of Africa (row 7) results from an unusually small increase in evaporation in the fixed H_2O experiment. A full analysis of the reason for this small increase is beyond the scope of this paper.

While the effect of water vapor feedback on the evaporation increase exhibits no systematic spatial-scale dependence, unlike the internal evaporation variability case, the two cases are similar in that the precipitation and evaporation ratios can differ substantially at all scales smaller than the global scale. As noted in section 4, this is due to the fact that at smaller scales there is no simple balance between evaporation and precipitation. Since moisture anomalies may be easily advected by the atmospheric circulation, the precipitation change in one region draws on the evaporation change in many other regions, guaranteeing that its magnitude (and possibly sign) will be different than the local evaporation increase. This effect is readily seen by examining the case of Australia (row 10). Here evaporation increases of differing magnitudes take place in both experiments; however, while precipitation increases in the control case, it actually decreases by a small amount in the fixed H_2O. This serves to underline the importance of water vapor feedback not only to the global scale intensification of the hydrologic cycle but also to human-induced regional changes in the balance between evaporation and precipitation.

6. Summary and Discussion

In section 4 we showed that global-mean precipitation variability is larger in the unperturbed experiment with water vapor feedback than the experiment without. We also demonstrated that this difference in precipitation variability can be traced to a difference in evaporation variability. Then we diagnosed the reason for the difference in evaporation variability: In the control experiment, global-mean surface temperature anomalies are more than 3 times as effective in inducing global-mean evaporation anomalies as their fixed H_2O counterparts. Because water vapor affects downward longwave radiation so as to counteract the temperature-anomaly-induced changes in upward longwave radiation, there is virtually no change in net surface longwave radiation as surface temperature fluctuates in the control experiment. Latent heat fluxes therefore take on an important role in the damping of surface temperature anomalies. When water vapor feedback is absent, there is less anomalous downward flux to counteract the anomalous upward flux related to surface temperature fluctuations. Thus longwave radiation acts to damp surface temperature anomalies in the fixed H_2O experiment. This greatly reduces evaporative damping. We also noted in this section that while the interaction between longwave and water vapor does have a significant impact on the internally generated variations of the global hydrologic cycle, its effect decreases as spatial scales decrease, so water vapor feedback has only a very small impact on grid-scale evaporation and precipitation variability.

In section 5 we demonstrated the importance of water vapor feedback in the intensification of the hydrologic cycle in global warming. In the control global warming experiment, the global precipitation increase is nearly an order of magnitude larger than in the experiment without water vapor feedback. The cause of this difference is similar to the cause of the difference in precipitation variability in the unperturbed integrations. In the control case, CO_2-induced warming and the associated increase of tropospheric absolute humidity increase downward longwave radiation. In fact, the increase in downward longwave is so large that the net longwave radiation actually acts to heat the surface, in spite of the increase in upward longwave radiation that results from the higher temperature. To maintain surface heat balance, evaporation must increase, leading to a similar increase in precipitation. The increase in water vapor associated with a warmer climate does not change downward radiation in the fixed H_2O case. The change in net longwave is therefore dominated by the increase in upward radiation due to the temperature increase, and net longwave acts to cool the surface. This greatly reduces the need for cooling through enhanced evaporation, thereby greatly weakening the intensification of the hydrological cycle. The large difference in hydrologic cycle intensification between the experiments with and without water vapor feedback extends to smaller spatial scales: The impact of water vapor feedback does not weaken systematically as spatial scales decrease, unlike the internal variability case.

It is worth noting that the impact of water vapor feedback on internally generated hydrologic cycle variability is smaller than its impact on hydrologic cycle intensification in global warming: This is revealed by the fact that on a per degree Centigrade basis, water vapor feedback is responsible for a larger evaporation anomaly in the global warming case. From Figure 3 it is evident that the latent heat anomaly associated with a 1° internally generated global-mean temperature anomaly is 0.74 W m^{-2} larger in the control than in the fixed H_2O case. On the other hand, from Figure 5 the latent heat flux increase associated with a 1° global warming is 1.14 W m^{-2} larger in the control experiment than in its fixed H_2O counterpart.

The main reason for this difference is that water vapor feedback itself is stronger in the global warming context [*Hall and Manabe*, 1999]: This is because the global warming induced by an increase in CO_2 is relatively uniform throughout the troposphere, whereas a global-mean, internally generated surface temperature anomaly does not penetrate nearly as effectively into the troposphere. This is the case even in the lower troposphere, which is the part of the atmosphere most critical for the surface energy balance. For example, in the global warming case, the entire troposphere warms almost exactly as much as the surface, whereas in the unperturbed variability case, the regression between annual-mean, global-mean, tropospheric temperature and surface temperature falls

off from 1 to about 0.5 at 700 hPa. Since global-mean tropospheric relative humidity does not change markedly as global-mean surface temperature fluctuates in either the externally forced or internally generated case, this results in a stronger relationship between lower tropospheric water vapor and surface temperature in the global warming case. This difference is reflected in the relationship between global-mean surface temperature and downward longwave radiation at the surface, which we examined in both sections 4 and 5: Analyzing the unperturbed variability experiments, we found that the regression between the two variables was larger in the control case by 1.06 W m^{-2} °C^{-1} (see Table 1), whereas the increase in downward longwave radiation per degree surface warming in the global warming experiments was 1.76 W m^{-2} °C^{-1} larger in the control case. The effect of water vapor feedback on the relationship between latent heat flux and surface temperature is similarly larger in the global warming experiments.

These model results demonstrate the importance of water vapor feedback both for internal variations in global-mean precipitation and for greenhouse-gas-induced intensification of the hydrologic cycle. Even if the predictions of the model are not perfect in a quantitative sense, they imply that uncertainty regarding the strength of water vapor feedback leads to uncertainty not only of the temperature sensitivity of the real climate to an increase in greenhouse gases but also of the projected future increase in precipitation. Our study illustrates in a particularly direct and graphic way that accurate representations of the radiative effects of water vapor and the relationship between atmospheric water vapor and surface temperature are necessary to simulate both global-scale precipitation variability and intensification of the hydrologic cycle in global warming.

Acknowledgments. Alex Hall was supported by a NASA Earth System Science Fellowship while this research was carried out. A part of this work was conducted at the Geophysical Fluid Dynamics Laboratory of NOAA to which S. Manabe was affiliated. The authors are grateful to Ron Stouffer and Isaac Held, as well as two anonymous reviewers, for constructive criticism of the manuscript.

References

Bryan, K., Climate and the ocean circulation, III, The ocean model, *Mon. Weather Rev*., *97*, 806–827, 1969.

Bryan, K., and L. Lewis, A water mass model of the world ocean, *J. Geophys. Res*., *84*, 2503–2517, 1979.

Dickinson, R. E., et al., Climate processes, in *Intergovernment Panel on Climate Change: The Science of Climate Change*, pp. 191–228, Cambridge Univ. Press, New York, 1996.

Hall, A., and S. Manabe, The role of water vapor feedback in unperturbed climate variability and global warming, *J. Clim*., *12*, 2327–2346, 1999.

Kattenberg, A., et al., Climate models—projections of future climate, in *Climate Change 1995: The Science of Climate Change*, pp. 285–357, Cambridge Univ. Press, New York, 1996.

Manabe, S., and R. Wetherald, Thermal equilibrium of the atmosphere with a given distribution of relative humidity, *J. Atmos. Sci*., *24*, 241–259, 1967.

Manabe, S., and R. Wetherald, The effects of doubling CO_2 concentration on the climate of a general circulation model, *J. Atmos. Sci*., *32*, 3–15, 1975.

Manabe, S., R. J. Stouffer, M. Spelman, and K. Bryan, Transient responses of a coupled ocean-atmosphere model to gradual changes of atmospheric CO_2, part I, Annual-mean response, *J. Clim*., *4*, 785–817, 1991.

Marotzke, J., and P. Stone, Atmospheric transports, the thermohaline circulation, and flux adjustments in a simple coupled model, *J. Phys. Oceanogr*., *25*, 1350–1364, 1995.

Mitchell, J. F. B., C. A. Wilson, and W. M. Cunnington, On CO_2 climate sensitivity and model dependence of results, *Q. J. R. Meteorol. Soc*., *113*, 293–322, 1987.

Mitchell, J. F. B., et al., Equilibrium climate change—and its implications for the future, in *Climate Change 1995: The Science of Climate Change*, pp. 131–172, Cambridge Univ. Press, New York, 1990.

Pacanowski, R., K. Dixon, and A. Rosati, The G.F.D.L modular ocean model users guide, *GFDL Ocean Group Tech. Rep. 2*, Geophys. Fluid Dyn. Lab., Princeton, N. J., 1991.

Redi, M. H., Oceanic isopycnal mixing by coordinate rotation, *J. Phys. Oceanogr*., *12*, 1154–1158, 1982.

Sun, D. Z., and I. Held, A Comparison of modeled and observed relationships between interannual variations of water vapor and temperature, *J. Clim*., *9*, 665–675, 1996.

Tziperman, E., and K. Bryan, Estimating global air-sea fluxes from surface properties and from climatological flux data using an oceanic general circulation model, *J. Geophys. Res*., *98*, 22,629–22,644, 1993.

Wetherald, R., and S. Manabe, The effects of changing the solar constant on the climate of a general circulation model, *J. Atmos. Sci*., *32*, 2044–2059, 1975.

A. Hall, Lamont-Doherty Earth Observatory, Columbia University, Oceanography Bldg., Room 103, P.O. Box 1000, 61 Route 9W, Palisades, NY 10964-8000. (alexhall@rosie.ldeo.columbia.edu)

S. Manabe, Institute for Global Change Research/FRSGC, 7th Floor, Seavans Building-N, 1-2-1 Shibaura, Minato-ku, Tokyo 105-6791, Japan.

(Received January 20, 1999; revised November 1, 1999;
accepted November 10, 1999.)